



## Modeling selective local interactions with memory

Amanda Galante, Doron Levy\*

Department of Mathematics, University of Maryland, College Park, MD 20742, United States

Center for Scientific Computation and Mathematical Modeling (CSCAMM), University of Maryland, College Park, MD 20742, United States

### ARTICLE INFO

#### Article history:

Available online 7 November 2012

#### Keywords:

Phototaxis  
Reaction–diffusion master equation  
Collective motion  
Group dynamics

### ABSTRACT

Recently we developed a stochastic particle system describing local interactions between cyanobacteria. We focused on the common freshwater cyanobacteria *Synechocystis* sp., which are coccoidal bacteria that utilize group dynamics to move toward a light source, a motion referred to as phototaxis. We were particularly interested in the local interactions between cells that were located in low to medium density areas away from the front. The simulations of our stochastic particle system in 2D replicated many experimentally observed phenomena, such as the formation of aggregations and the quasi-random motion of cells. In this paper, we seek to develop a better understanding of group dynamics produced by this model. To facilitate this study, we replace the stochastic model with a system of ordinary differential equations describing the evolution of particles in 1D. Unlike many other models, our emphasis is on particles that selectively choose one of their neighbors as the preferred direction of motion. Furthermore, we incorporate memory by allowing persistence in the motion. We conduct numerical simulations which allow us to efficiently explore the space of parameters, in order to study the stability, size, and merging of aggregations.

© 2012 Elsevier B.V. All rights reserved.

### 1. Introduction

In a recent work we proposed a mathematical model of local interactions between cyanobacteria [1,2]. The goal of that work was to model the motion of the phototactic microorganism *Synechocystis* sp., which typically form aggregations before engaging in phototaxis, i.e., a motion towards light. Over time, phototaxis results in the formation of finger-like structures in the direction of the light source [3,4]. We focused our study on the dynamics of cells after they become sufficiently excited to engage in movement but are not sufficiently “motivated” to migrate toward the light. Simulations of our 2D stochastically interacting particle model produced results which were consistent with the experimental observations. Our model assumptions included the possibility of persistence with memory as well as a motion toward a randomly selected neighboring bacteria.

Interactions between animal and cellular agents have been modeled extensively. One celebrated example is the Couzin–Vicsek model of flocking (and its many extensions) which allows individual agents, such as fish or birds, to be repelled by near neighbors, align with the average directional heading of not-so-near neighbors, and be attracted to far neighbors [5,6].

Some features of the model have been subjected to thorough mathematical analysis; for example see [7]. The dynamical system presented by Cucker and Smale models the development of a consensus in populations lacking central direction [8,9]. This model has also been thoroughly analyzed, for example see [10]. Numerous similar flocking and schooling models have been developed for various self-propelling agents such as birds and fish, e.g. [11–15]. Many of these models consider the sum of forces on each individual agent, due to neighboring agents, the directional heading of each agent, and any other external forces. In comparison to these works, the model we discuss here is a non-physical model. Particles randomly select a direction toward only one of the neighboring agents, instead of moving in response to an averaged force field.

A related phenomenon, chemotaxis, i.e., motion of cells toward a chemoattractant, has been extensively studied by mathematicians in recent decades, starting with the celebrated works of Patlak, Keller and Segel [16,17]. For completeness, we refer the interested reader to the following papers and to the references therein [18–22]. Many of the works on chemotaxis study the aggregations of cells and the possible blowup in the limit of high concentrations. In our case, experimentally, aggregations correspond to groups of 3–10 cells which can come together, may occasionally move as a unit, and can dissociate. This is a very different dynamics than what is typically observed in chemotaxis.

Compared with chemotaxis and flocking models, phototaxis has not been as extensively studied by the mathematical modeling community. Relatively few models of phototaxis have been developed, for example see [23,24]. These models do not focus

\* Corresponding author at: Department of Mathematics, University of Maryland, College Park, MD 20742, United States.

E-mail addresses: [agalante@cscamm.umd.edu](mailto:agalante@cscamm.umd.edu) (A. Galante), [dlevy@math.umd.edu](mailto:dlevy@math.umd.edu) (D. Levy).

on the intercellular group dynamics. Other recent works include an agent-based model considering cell interactions due to the transmission of light by individual cells [25] and ODE and statistical models examining rotational properties of an algal colony of biflagellar *V. Carteri* cells [26]. Additional works on phototaxis include [27,4,28–30], for which the primary focus was on modeling the initiation of the movement toward light and the resulting migration of the bacterial colony toward light (including the modeling of the finger formation). Absent from these works was a description of the observed dynamics in regions of low to medium cell density in which cells tend to move in a quasi-random pattern of motion towards neighboring cells, without any observable bias in the direction of motion due to the light source. This question was addressed in two recent papers [1,2] in which we presented and studied a 2D model of stochastically interacting particles. Simulations of the model produced results that were consistent with experimental data in low to medium cell densities.

In this paper we seek to develop a better understanding of the dynamics produced by the models in [1,2]. To address this goal, we consider a one-dimensional version of our stochastic 2D model. Starting from a set of basic rules of motion, we develop a reaction–diffusion master equation (RDME), from which we derive a system of ODEs describing the cell populations along an indexed number line. This approach follows Baker et al. who focused on a variety of signaling patterns and boundary conditions to study cell migration on growing domains [31].

The structure of this paper is as follows. In Section 2 we derive a system of ODEs from a 1D version of our 2D model from [1,2]. In Section 3 we compare simulations of our stochastic 1D particle system and the new system of ODEs to illustrate the strengths and weaknesses of each model. The simulations illustrate that the ODE system does in fact capture many of the key features that were observed with the stochastic particle system in [1,2], including the experimentally observed formation of aggregations and merging aggregations. Furthermore, the ODEs replicate the approximate number, location, and width of aggregations produced by the stochastic system. We also utilize the system of ODEs to explore the parameter space, which we can now do more thoroughly because solving the system of ODEs requires less computational resources than solving the corresponding stochastic particle system. Section 4 contains an extended discussion of the results. Concluding remarks are given in Section 5.

## 2. Local interaction model in one dimension

In [1,2], we developed a model of local interactions of *Synechocystis* sp. which assumes that particles move in two dimensions according to the following rules, depicted in Fig. 1:

- (i) Particles can persist in their motion, that is, move straight without changing their direction for a certain duration of time.
- (ii) Particles can start and stop, at time intervals of varying length.
- (iii) Particles can change direction. When particles change direction, we assume that they choose to move towards one of their neighbors, within some fixed radius.

We assign a probability to each event. Persistence occurs with probability  $a$ , stopping occurs with probability  $b$ , and movement toward a selected neighbor occurs with probability  $(1 - a - b)/N_n$  where  $N_n$  is the number of neighbors located within the fixed radius. Simulations of this model were qualitatively very similar to experimentally observed behaviors of *Synechocystis* sp.; however, this 2D agent-based model is difficult to analyze and to characterize the motion for different parameter sets, as agent-based simulations are relatively inefficient.

To derive a one-dimensional version of the agent-based model from [1,2], we consider a set of  $N$  particles, each with a given initial

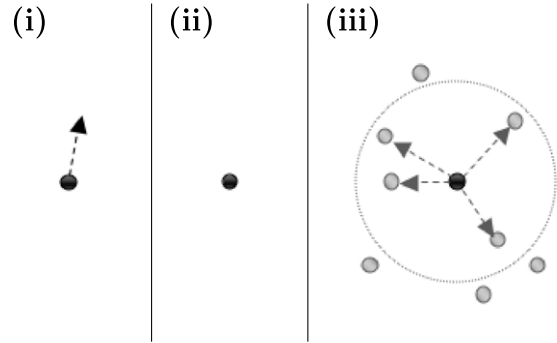


**Fig. 1.** Local interaction model. Model particles can exhibit (i) persistence, (ii) stationary behavior, and (iii) movement toward neighboring cells within a fixed radius.

position and initial preferred direction. Let the position of each particle  $i$  at time  $t$  be denoted by  $x_i(t)$ , where  $x_i(t) \in \{1, 2, \dots, k\}$  for  $i = 1, \dots, N$ . In this way we have  $N$  particles in  $k$  bins along a line.

Assume that all particles move at a fixed speed  $v$ , so that at every time step  $\Delta t$ , if a particle moves, the displacement is  $\Delta x = v\Delta t$ . At every time-step, there are three possibilities: (i) a particle can persist in its previous direction of motion with probability  $a$ , (ii) a particle can remain stationary with probability  $b$ , or (iii) a particle can choose a new direction, in which case the new direction is either right or left, one of which must be its previous direction. Just as in [1,2], we allow particles to sense neighbors within a given distance and the probability associated with motion (iii) depends on the location of neighboring particles. Note that in the 1D case, the model becomes a system of right-moving and left-moving particles on a line, as moving particles can only move to the right or to the left of their current positions. When a particle moves to the right, its position  $x_i(t)$  is increased by  $\Delta x$ . When a particle steps to the left, its position  $x_i(t)$  is decreased by  $\Delta x$ . Scaling  $\Delta t = 1$ , we have  $x_i(t + 1)$

$$= \begin{cases} x_i(t) + p_i(t), & \text{with probability } a, \\ x_i(t), & \text{with probability } b, \\ x_i(t) + \Delta x, & \text{with probability } (1 - a - b) \frac{v_i^+}{v_i^+ + v_i^-}, \\ x_i(t) - \Delta x, & \text{with probability } (1 - a - b) \frac{v_i^-}{v_i^+ + v_i^-}. \end{cases} \quad (1)$$

Here  $p_i(t)$  is the last direction in which the particle moved (i.e., either  $\Delta x$  or  $-\Delta x$ ). The number of particles to the right of bin  $x_i$  that can be sensed by particle  $i$  is

$$v_i^+ = \sum_{m=1}^D \sum_{j=1}^N \delta_{x_j, x_i + m\Delta x}, \quad (2)$$

and the number of particles to the left of bin  $x_i$  that can be sensed by particle  $i$  is

$$v_i^- = \sum_{m=1}^D \sum_{j=1}^N \delta_{x_j, x_i - m\Delta x}. \quad (3)$$

Here,  $\delta_{x_i, x_j}$  is the Kronecker delta function; that is,  $\delta_{x_i, x_j}$  is 1 if  $x_i = x_j$ , and 0 otherwise. In this way, the probabilities associated with choosing the direction of motion reduce to the weights of neighboring particles. Note that the discrete stochastic system (1) is not Markovian; the position at time  $t + 1$  depends on the position at time  $t - 1$ , not just the position at time  $t$ . We depict this system in Fig. 2.

For this setup, a variety of boundary conditions can be considered. In this paper, we consider a fixed number of particles on a fixed interval with periodic boundary conditions.

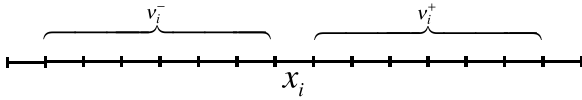


**Fig. 2.** A number line illustrating the bin position  $x_i$  of particle  $i$  with detectable neighbors being the total number of particles which fall in the regions indicated by  $v_i^+$  and  $v_i^-$ . In this particular image, the neighbor detection distance is  $D = 6$ .

**2.1. Derivation of the reaction–diffusion master equation (RDME)**

We begin our derivation of a reaction–diffusion master equation by considering the number of particles in each bin, as opposed to the position of each particle; the former is more practical for systems with large numbers of particles. The number of particles  $n_i(t)$  in bin  $i$  at time  $t$  is given by

$$n_i(t) = \sum_{j=1}^N \delta_{x_j(t), i\Delta x}. \tag{4}$$

Suppose that the particles are distributed between  $k$  bins. The number of particles in bins  $i = 1, \dots, k$  is given by the vector:

$$\vec{n} = [n_1, n_2, \dots, n_i, \dots, n_k]. \tag{5}$$

Note that the vector  $\vec{n}$  and each of its components  $n_i$  are functions of time  $t$ , which has been suppressed here for the sake of brevity.

We can now use Eqs. (2)–(4) to rewrite our expressions for the number of detectable neighboring particles in each direction:  $v_i^- = \sum_{m=1}^D n_{i-m}$  and  $v_i^+ = \sum_{m=1}^D n_{i+m}$ . To simplify the notations, we define neighbor-weighted probabilities  $c_i^r = (1 - a - b)v_i^+ / (v_i^- + v_i^+)$  and  $c_i^l = (1 - a - b)v_i^- / (v_i^- + v_i^+)$ , which are the probabilities of a particle choosing to move to the right or the left, respectively.

We distinguish between four types of particles: right-moving, left-moving, right-stationary, and left-stationary. A particle is considered to be right- (or left-) stationary if it moved to the right (or to the left) to enter the current bin but remained stationary during the previous time-step. Note that a stationary particle remembers its previous direction. This memory allows for continued persistence in the preferred direction when the particle resumes moving.

Let  $r_i(t)$  be the number of particles that moved into bin  $i$  from bin  $i - 1$  during the previous time-step. Let  $r_i^s(t)$  denote the number of particles at time  $t$  which have become stationary, but previously moved to the right from bin  $i - 1$  to  $i$ . Similarly, we define  $l_i(t)$  as the left-moving particles in bin  $i$  at time  $t$ , which moved left from bin  $i + 1$  into bin  $i$  during the previous time-step. Finally, we define  $l_i^s(t)$  to be the number of particles in bin  $i$  at time  $t$  which moved left in their most recent transition between bins, but remained stationary during the previous time-step. We assume that particles become (or remain) stationary with probability  $b$ . The governing set of rules are shown in Fig. 3.

In order to write a reaction–diffusion master equation (RDME) describing how these populations evolve probabilistically in time, we consider the probability density function  $P(\vec{r}, \vec{l}, \vec{r}^s, \vec{l}^s, t)$  describing the likelihood of a system to be in a given state  $\{\vec{r}, \vec{l}, \vec{r}^s, \vec{l}^s, t\}$ . We note that for transitions between these four populations, there is the additional possibility of particles becoming stationary or moving after having been stationary. Accordingly, the equation is written as

$$\frac{\partial P}{\partial t}(\vec{r}, \vec{l}, t) = \sum_{i=1}^{k-1} \left[ \underbrace{\left( \text{Probability that a particle moves out of bin } i \text{ to the right to enter the state } \{\vec{r}, \vec{l}, \vec{r}^s, \vec{l}^s, t\} \right)}_{\textcircled{1}} - \underbrace{\left( \text{Probability that a particle moves out of bin } i \text{ to the right to leave the state } \{\vec{r}, \vec{l}, \vec{r}^s, \vec{l}^s, t\} \right)}_{\textcircled{2}} \right]$$

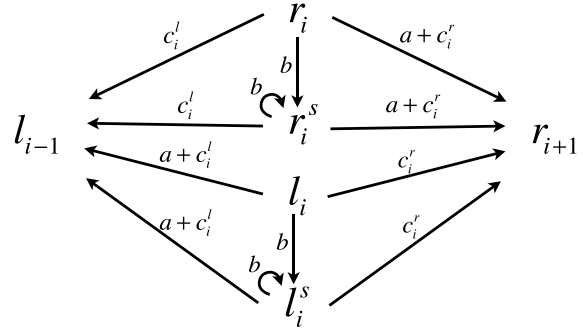


**Fig. 3.** The options for the motion of particles out of a right-moving  $r_i$  or left-moving  $l_i$  populations in bin  $i$ , with associated probabilities for a system of particles which are either right-moving or left-moving and have the ability to become stationary with memory of a preferred direction. Not shown are the sources of right-moving and left-moving particles. The source of particles in  $r_i$  is all particle types in bin  $i - 1$ , and the source of particles in  $l_i$  is all particle types in bin  $i + 1$ . The associated probabilities of these sources can be extracted from the diagram. The probability  $a$  denotes persistence, the probability  $b$  denotes becoming (or staying) stationary and the probabilities  $c_i^r$  and  $c_i^l$  denote choosing a direction based on neighbor weights.

$$+ \sum_{i=2}^k \left[ \underbrace{\left( \text{Probability that a particle moves out of bin } i \text{ to the left to enter the state } \{\vec{r}, \vec{l}, \vec{r}^s, \vec{l}^s, t\} \right)}_{\textcircled{3}} - \underbrace{\left( \text{Probability that a particle moves out of bin } i \text{ to the left to leave the state } \{\vec{r}, \vec{l}, \vec{r}^s, \vec{l}^s, t\} \right)}_{\textcircled{4}} \right] + \sum_{i=1}^k \left( \text{Probability that a particle in bin } i \text{ becomes stationary to enter or leave the state } \{\vec{r}, \vec{l}, \vec{r}^s, \vec{l}^s, t\} \right)_{\textcircled{5}} + \underbrace{\text{Boundary terms.}}_{\textcircled{6}} \tag{6}$$

To address each of the terms in (6), we need to define particle-transposing operators. We define these operators so that they each act on the state of the system,  $\{\vec{r}, \vec{l}, \vec{r}^s, \vec{l}^s\}$ . In Table 1, we define all operators, but only show the populations which are directly affected by the operator. All other populations remain whatever they are in the state  $\{\vec{r}, \vec{l}, \vec{r}^s, \vec{l}^s\}$ , as this table accounts for all possible translations which are one particle movement away from the state of interest.

Using the operators in Table 1 and probabilistic rates of transitioning to the right or left, we are able to determine each component of the RDME (6). For  $\textcircled{1}$ , we want to account for the probability of a particle in bin  $i$  moving to the right to enter state  $\{\vec{r}, \vec{l}, \vec{r}^s, \vec{l}^s, t\}$ . The rate at which a right-moving particle moves right is  $a + c_i^r$ . Note that  $c_i^r$  depends on the position of other particles and so we need to be a little more careful in handling this term. For a particle to move out of bin  $i$  to the right so that the new state is  $\{\vec{r}, \vec{l}, \vec{r}^s, \vec{l}^s, t\}$ , the particles must be arranged as in Fig. 4. To calculate the neighbor-dependent weight which would allow a particle in bin  $i$  to move to the right, we sum over the neighbors to the right within neighbor detection distance  $D$  and normalize by dividing by the total number of neighbors within neighbor detection distance  $D$ . If we use the previous formula  $v_i^+ = \sum_{j=1}^D n_{i+j}$  with values from the current state, the number of neighbors to the right of bin  $i$  is exactly  $v_i^+ - 1$ . The number of neighbors to the left,  $v_i^-$ , has not changed. Hence, for this setup, the weight for moving to the right is  $(v_i^+ - 1) / (v_i^+ + v_i^- - 1)$ . We can now calculate the probability of a right-moving particle moving to the right out of bin  $i$ . The probability that the particles

**Table 1**

Definitions of particle-transposition operators acting on  $\{\vec{r}, \vec{l}, \vec{r}^s, \vec{l}^s\}$ . The first subscript indicates the bin on which the operator is acting. The second subscript indicates the population type. The superscript indicates the direction in which that particle is moving, right (+), left (−), or (s) if the particle is becoming stationary.

Operator	Result
$J_{i,r}^+$	$[\dots, r_i + 1, r_{i+1} - 1, \dots]$
$J_{i,r^s}^+$	$[\dots, r_{i+1} - 1, \dots, r_i^s + 1, \dots]$
$J_{i,l}^+$	$[\dots, r_{i+1} - 1, \dots, l_i + 1, \dots]$
$J_{i,l^s}^+$	$[\dots, r_{i+1} - 1, \dots, l_i^s + 1, \dots]$
$J_{i,r}^-$	$[\dots, r_i + 1, \dots, l_{i-1} - 1, \dots]$
$J_{i,r^s}^-$	$[\dots, l_{i-1} - 1, \dots, r_i^s + 1, \dots]$
$J_{i,l}^-$	$[\dots, l_{i-1} - 1, l_i + 1, \dots]$
$J_{i,l^s}^-$	$[\dots, l_{i-1} - 1, \dots, l_i^s + 1, \dots]$
$J_{i,r}^s$	$[\dots, r_i + 1, \dots, r_i^s - 1, \dots]$
$J_{i,l}^s$	$[\dots, l_i + 1, \dots, l_i^s - 1, \dots]$

Right-moving particles	...	$r_{i-1}$	$r_i + 1$	$r_{i+1} - 1$	$r_{i+2}$	...
Left-moving particles	...	$l_{i-1}$	$l_i$	$l_{i+1}$	$l_{i+2}$	...
Right-stationary particles	...	$r_{i-1}^s$	$r_i^s$	$r_{i+1}^s$	$r_{i+2}^s$	...
Left-stationary particles	...	$l_{i-1}^s$	$l_i^s$	$l_{i+1}^s$	$l_{i+2}^s$	...
Total	...	$n_{i-1}$	$n_i + 1$	$n_{i+1} - 1$	$n_{i+2}$	...

**Fig. 4.** Setup of particles for  $J_{i,r}^+[\vec{r}, \vec{l}, \vec{r}^s, \vec{l}^s]$ .

are in the configuration shown in Fig. 4 is  $P(J_{i,r}^+[\vec{r}, \vec{l}, \vec{r}^s, \vec{l}^s], t)$ . The number of particles which could move to the right is  $r_i + 1$ . The rate at which these particles could move to the right is the sum of the persistence probability and the neighbor-weight probability, i.e.,  $a + (1 - a)(v_i^+ - 1)/(v_i^+ + v_i^- - 1)$ . The product of these three expressions is the first term in item ①.

Another way for a particle to be located in bin  $i$  and move to the right is for a left-moving particle to choose to move to the right. This setup is shown in Fig. 5. Note that the total number of particles in each bin is the same and hence this setup produces the same neighbor weight as for a right-moving particle choosing to move to the right. Similarly, one can construct figures for right-stationary and left-stationary particles moving to the right. The neighbor weights are the same for all four cases. With these four setups, we have accounted for all possible ways that an extra particle to be present in bin  $i$  and move to the right to bin  $i + 1$  with the system entering the state  $\{\vec{r}, \vec{l}, \vec{r}^s, \vec{l}^s, t\}$ . Accordingly, the term ① in Eq. (6) is given by

$$\begin{aligned} \textcircled{1} : & \left[ a + (1 - a) \frac{v_i^+ - 1}{v_i^+ + v_i^- - 1} \right] (r_i + 1) P(J_{i,r}^+[\vec{r}, \vec{l}, \vec{r}^s, \vec{l}^s], t) \\ & + \left[ (1 - a) \frac{v_i^+ - 1}{v_i^+ + v_i^- - 1} \right] (l_i + 1) P(J_{i,l}^+[\vec{r}, \vec{l}, \vec{r}^s, \vec{l}^s], t) \\ & + \left[ a + (1 - a) \frac{v_i^+ - 1}{v_i^+ + v_i^- - 1} \right] (r_i^s + 1) P(J_{i,r^s}^+[\vec{r}, \vec{l}, \vec{r}^s, \vec{l}^s], t) \\ & + \left[ (1 - a) \frac{v_i^+ - 1}{v_i^+ + v_i^- - 1} \right] (l_i^s + 1) P(J_{i,l^s}^+[\vec{r}, \vec{l}, \vec{r}^s, \vec{l}^s], t). \end{aligned}$$

To derive ② in Eq. (6), we need to account for particles that are present in bin  $i$ , move right to the bin  $i + 1$ , and leave the state  $\{\vec{r}, \vec{l}, \vec{r}^s, \vec{l}^s, t\}$ . In this setup, the neighbor-weight probability  $c_i^+$  is

Right-moving particles	...	$r_{i-1}$	$r_i$	$r_{i+1} - 1$	$r_{i+2}$	...
Left-moving particles	...	$l_{i-1}$	$l_i + 1$	$l_{i+1}$	$l_{i+2}$	...
Right-stationary particles	...	$r_{i-1}^s$	$r_i^s$	$r_{i+1}^s$	$r_{i+2}^s$	...
Left-stationary particles	...	$l_{i-1}^s$	$l_i^s$	$l_{i+1}^s$	$l_{i+2}^s$	...
Total	...	$n_{i-1}$	$n_i + 1$	$n_{i+1} - 1$	$n_{i+2}$	...

**Fig. 5.** Setup of particles for  $J_{i,l}^+[\vec{r}, \vec{l}, \vec{r}^s, \vec{l}^s]$ .

exactly what we expect:  $(1 - a)(v_i^+)/(v_i^+ + v_i^-)$ . Again we attain the expressions in item ② by taking the product of the probability of the system being set up in the appropriate state,  $P(\vec{r}, \vec{l}, \vec{r}^s, \vec{l}^s, t)$ , the number of particles available to move, either  $r_i, l_i, r_i^s$ , or  $l_i^s$ , and the probabilistic rate of particles moving to the right. This rate is the neighbor weight probability, with the persistence probability  $a$  added for right-moving and right-stationary particles. Hence,

$$\begin{aligned} \textcircled{2} : & \left[ a + (1 - a) \frac{v_i^+}{v_i^+ + v_i^-} \right] r_i P(\vec{r}, \vec{l}, \vec{r}^s, \vec{l}^s, t) \\ & + \left[ (1 - a) \frac{v_i^+}{v_i^+ + v_i^-} \right] l_i P(\vec{r}, \vec{l}, \vec{r}^s, \vec{l}^s, t) \\ & + \left[ a + (1 - a) \frac{v_i^+}{v_i^+ + v_i^-} \right] r_i^s P(\vec{r}, \vec{l}, \vec{r}^s, \vec{l}^s, t) \\ & + \left[ (1 - a) \frac{v_i^+}{v_i^+ + v_i^-} \right] l_i^s P(\vec{r}, \vec{l}, \vec{r}^s, \vec{l}^s, t). \end{aligned}$$

For item ③ in (6), we consider all terms where particles move left, with the system entering the state  $\{\vec{r}, \vec{l}, \vec{r}^s, \vec{l}^s, t\}$ :

$$\begin{aligned} \textcircled{3} : & \left[ (1 - a) \frac{v_i^- - 1}{v_i^+ + v_i^- - 1} \right] (r_i + 1) P(J_{i,r}^-[\vec{r}, \vec{l}, \vec{r}^s, \vec{l}^s], t) \\ & + \left[ a + (1 - a) \frac{v_i^- - 1}{v_i^+ + v_i^- - 1} \right] (l_i + 1) P(J_{i,l}^-[\vec{r}, \vec{l}, \vec{r}^s, \vec{l}^s], t) \\ & + \left[ (1 - a) \frac{v_i^- - 1}{v_i^+ + v_i^- - 1} \right] (r_i^s + 1) P(J_{i,r^s}^-[\vec{r}, \vec{l}, \vec{r}^s, \vec{l}^s], t) \\ & + \left[ a + (1 - a) \frac{v_i^- - 1}{v_i^+ + v_i^- - 1} \right] (l_i^s + 1) P(J_{i,l^s}^-[\vec{r}, \vec{l}, \vec{r}^s, \vec{l}^s], t). \end{aligned}$$

For item ④ in (6), we consider all terms where particles move left, with the system leaving the state  $\{\vec{r}, \vec{l}, \vec{r}^s, \vec{l}^s, t\}$ :

$$\begin{aligned} \textcircled{4} : & \left[ (1 - a) \frac{v_i^-}{v_i^+ + v_i^-} \right] r_i P(\vec{r}, \vec{l}, \vec{r}^s, \vec{l}^s, t) \\ & + \left[ a + (1 - a) \frac{v_i^-}{v_i^+ + v_i^-} \right] l_i P(\vec{r}, \vec{l}, \vec{r}^s, \vec{l}^s, t) \\ & + \left[ (1 - a) \frac{v_i^-}{v_i^+ + v_i^-} \right] r_i^s P(\vec{r}, \vec{l}, \vec{r}^s, \vec{l}^s, t) \\ & + \left[ a + (1 - a) \frac{v_i^-}{v_i^+ + v_i^-} \right] l_i^s P(\vec{r}, \vec{l}, \vec{r}^s, \vec{l}^s, t). \end{aligned}$$

For item ⑤ in (6), we account for the probability of moving particles becoming stationary, both to enter and exit the state  $\{\vec{r}, \vec{l}, \vec{r}^s, \vec{l}^s, t\}$ . Particles become stationary with probabilistic rate  $b$ . Hence

$$\textcircled{5} : b(r_i + 1)P(J_{i,r}^s[\vec{r}, \vec{l}, \vec{r}^s, \vec{l}^s], t) + b(l_i + 1)P(J_{i,l}^s[\vec{r}, \vec{l}, \vec{r}^s, \vec{l}^s], t) - b[r_i^s + l_i^s]P(\vec{r}, \vec{l}, \vec{r}^s, \vec{l}^s, t).$$

Finally, the boundary terms  $\textcircled{6}$  in Eq. (6) take an obvious form in the case of periodic boundary conditions. Proper adjustments should be made for other types of boundary conditions.

## 2.2. Deriving a system of ODEs

We define the expected value of each population, e.g.

$$R_i = \langle r_i \rangle = \sum_{\vec{r}} \sum_{\vec{l}} \sum_{\vec{r}^s} \sum_{\vec{l}^s} r_i P(\vec{r}, \vec{l}, \vec{r}^s, \vec{l}^s, t). \quad (7)$$

Using this definition, taking the derivative with respect to time, substituting the RDME as appropriate and reindexing many of the summations, we obtain a new system of ODEs that models the average behavior of the system. For further detail on this approach we refer to [32]. We denote the transition rates with  $T$ .

The average behavior of the right-moving particles in bin  $i$ ,  $R_i$ , consists of particles entering from bin  $i-1$  and leaving either to the right, to the left, or to the stationary compartment. Consequently:

$$\frac{dR_i}{dt} = \langle r_{i-1} T_{i-1}^+ \rangle + \langle l_{i-1} T_{i-1}^+ \rangle + \langle r_{i-1}^s T_{i-1}^+ \rangle + \langle l_{i-1}^s T_{i-1}^+ \rangle - \langle r_i T_i^+ \rangle - \langle r_i T_i^- \rangle - \langle r_i T_i^s \rangle. \quad (8)$$

Similarly, the average behavior of the left-moving particles in slot  $i$ ,  $L_i$  consists of particles entering from bin  $i+1$  and leaving either to the right, to the left, or to the stationary compartment:

$$\frac{dL_i}{dt} = \langle r_{i+1} T_{i+1}^- \rangle + \langle l_{i+1} T_{i+1}^- \rangle + \langle r_{i+1}^s T_{i+1}^- \rangle + \langle l_{i+1}^s T_{i+1}^- \rangle - \langle l_i T_i^+ \rangle - \langle l_i T_i^- \rangle - \langle l_i T_i^s \rangle. \quad (9)$$

The right-stationary population in bin  $i$ ,  $R_i^s$ , increases as right-moving particles becoming stationary and decreases as the stationary particles leave to the left or the right:

$$\frac{dR_i^s}{dt} = \langle r_i T_i^s \rangle - \langle r_i^s T_i^+ \rangle - \langle r_i^s T_i^- \rangle. \quad (10)$$

The left-stationary population in bin  $i$ ,  $L_i^s$ , increases as left-moving particles becoming stationary and decreases as the stationary particles leave to the left or the right:

$$\frac{dL_i^s}{dt} = \langle l_i T_i^s \rangle - \langle l_i^s T_i^+ \rangle - \langle l_i^s T_i^- \rangle. \quad (11)$$

The transition rate  $T_{r_i}^+$  is the ‘rate of right-moving, or right-stationary, particles moving to the right’ and the transition rate  $T_{l_i}^-$  is the ‘rate of left-moving, or left-stationary, particles moving to the left’. Similarly, the transition rate  $T_{r_i}^-$  is the ‘rate of right-moving, or right-stationary, particles moving to the left’ and the transition rate  $T_{l_i}^+$  is the ‘rate of left-moving, or left-stationary, particles moving to the right’. In this way, the transition rates  $T_{r_i}^+$ ,  $T_{l_i}^+$ ,  $T_{l_i}^-$  take the following values:

$$T_{r_i}^+ = c_i^r + a, \quad (12)$$

$$T_{l_i}^+ = c_i^r, \quad (13)$$

$$T_{l_i}^- = c_i^l + a, \quad (14)$$

$$T_{r_i}^- = c_i^l, \quad (15)$$

where  $c_i^r = (1-a-b)v_i^+ / (v_i^- + v_i^+)$  and  $c_i^l = (1-a-b)v_i^- / (v_i^- + v_i^+)$ . Note that the rate at which particles move to the left or to

the right depends on whether a particle is left-moving or right-moving. We define the transition rate for particles going from a moving compartment to a stationary compartment as:

$$T_{r_i}^s = T_{l_i}^s = b. \quad (16)$$

Using the expressions for transition rates, we can simplify some of the expected value operators. The population of right-moving particles  $R_i$  simplifies to a system with right-moving and stationary particles in bin  $i-1$  persisting into bin  $i$  and all particles in bin  $i-1$  moving to the right with a neighbor-weighted probability  $c_{i-1}^r$ . Additionally, all right-moving particles leave the system at every time step, either by persisting, becoming stationary, or choosing to move toward a neighboring bin:

$$\frac{dR_i}{dt} = a(R_{i-1} + R_{i-1}^s) + \langle n_{i-1} c_{i-1}^r \rangle - R_i. \quad (17)$$

The population of right-stationary particles  $R_i^s$  consists of particles in  $R_i$  becoming stationary with stopping rate  $b$  and leaving the stationary population with rate  $1-b$ :

$$\frac{dR_i^s}{dt} = bR_i - (1-b)R_i^s. \quad (18)$$

The population of left-moving particles  $L_i$  simplifies to a system with left-moving and stationary particles in bin  $i+1$  persisting into bin  $i$  with rate  $a$  and all particles in bin  $i+1$  moving to the left with a neighbor-weighted probability  $c_{i+1}^l$ . Additionally, all left-moving particles leave the system at every time step, either by persisting, by becoming stationary, or by choosing to move toward a neighboring slot:

$$\frac{dL_i}{dt} = a(L_{i+1} + L_{i+1}^s) + \langle n_{i+1} c_{i+1}^l \rangle - L_i. \quad (19)$$

The population of left-stationary particles  $L_i^s$  consists of particles in  $L_i$  becoming stationary with stopping rate  $b$  and leaving the stationary population with rate  $1-b$ :

$$\frac{dL_i^s}{dt} = bL_i - (1-b)L_i^s. \quad (20)$$

Note that the system (17)–(20) conserves the total number of particles in the system. We can see this by summing the differential equations (17)–(20) over all bins and population types. In our simulations, when a particle has no neighbors, we set the neighbor-weight to zero to avoid division by zero. This does not affect the conservative nature of the system. This is typically not relevant at high particle densities but can be important as aggregations form, leaving sections of empty bins.

## 3. Simulations

The solution of the system of ODEs (17)–(20) is simulated with various initial conditions and periodic boundary conditions. Observe that the ODEs (17)–(20) contain unresolved expected value terms. To deal with these terms in our simulations, we approximate each expected value by the sum, product and quotient of the expected value of each term contained therein; that is, we drop the expected value operator and replace each term with its expected value. For instance,  $\langle r_i r_{i-1} \rangle$  is estimated by  $R_i R_{i-1}$ . We do this in order to expedite computation time and eliminate the need to calculate the probability density function  $P(\vec{r}, \vec{l}, \vec{r}^s, \vec{l}^s, t)$  for all possible particle number and time combinations.

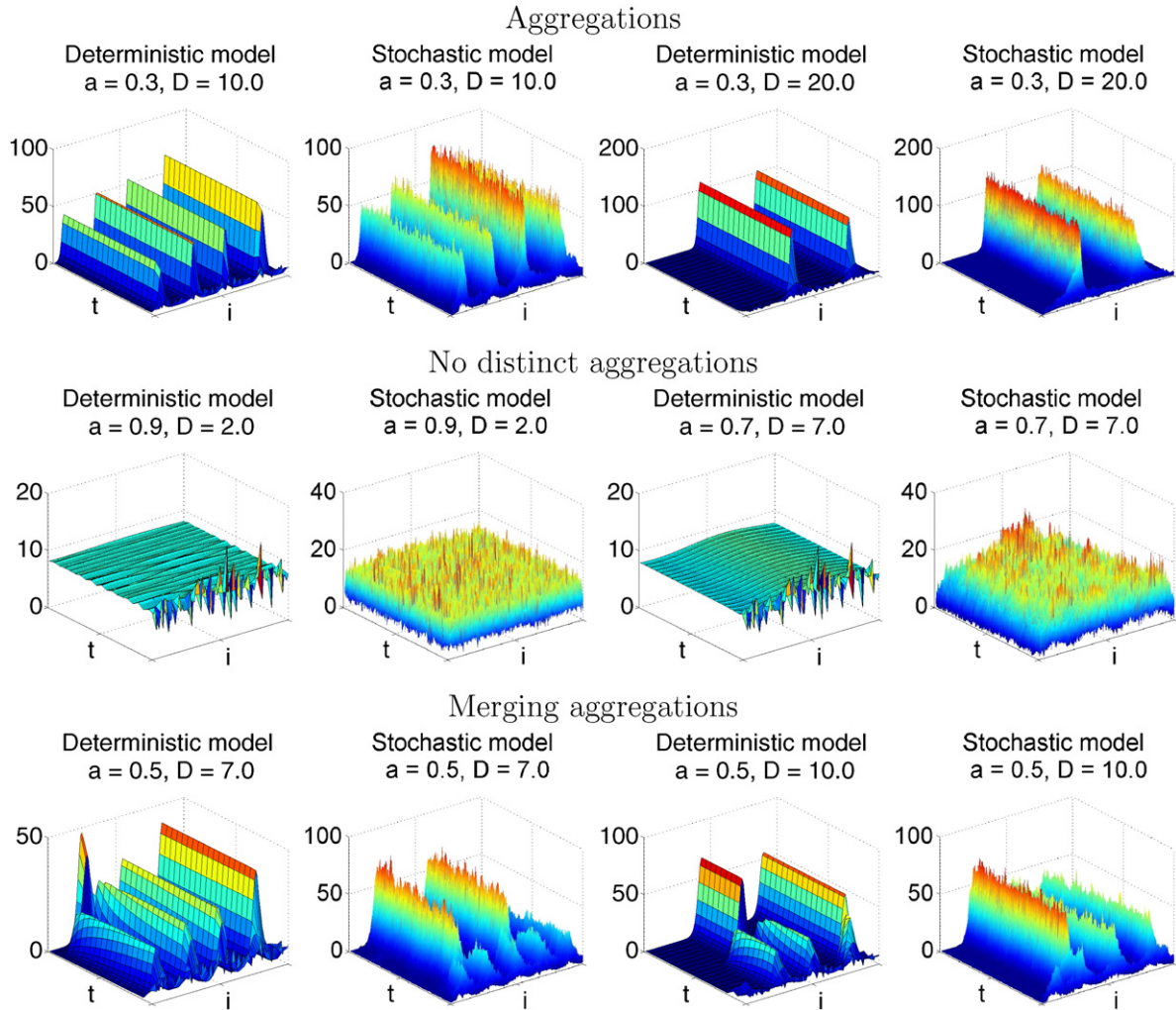


**Fig. 6.** A comparison of the stochastic particle system to the deterministic ODE for different scenarios: forming aggregations, the absence of aggregations, and merging aggregations. The parameters  $a$ , the persistence probability,  $D$ , the neighbor detection distance, and the initial data are identical in each case. The parameters  $a$  and  $D$  are varied as indicated above each plot to capture the different scenarios. For each of these images, the stopping probability  $b$  is 0.1 and the number of bins  $k$  is 100. On these 3D images, the  $i$ -axis is for bin number, from 1 to 100, the  $t$ -axis is for time, from 1 to 1000, and the vertical  $z$ -axis is for particle number.

### 3.1. Comparing the ODEs to the stochastic particle model

Our first numerical simulation compares the ODEs with the stochastic particle model. Our results are shown in Figs. 6 and 7. In both figures, we demonstrate three different observed patterns in order to show how the ODE model (17)–(20) can replicate the patterns obtained with the stochastic particle system (1). The three patterns shown are the formation of aggregations of particles, the lack of aggregations, and the formation of aggregations that merge. In Fig. 6, we show three-dimensional surface plots illustrating the number of particles in 100 bins from time 0 to 1000. In Fig. 7, we offer the same simulations as in Fig. 6, except that the number of particles in every bin is only portrayed at the final time 1000. In most simulations, we do not display numbers along certain axes to aid in visual discernment. In Fig. 6 and all other surface plots, the  $i$ -axis varies from 0 (at the left) to 100 (at the right) and the  $t$ -axis ranges from 0 (at the front) to 1000 (at the back). In Fig. 7 and all other 2D plots, the time is fixed at 1000 and the  $i$ -axis ranges from 0 (at the left) to 100 (at the right). The vertical axis in each case is for  $M_i(t)$ , the expected total number of particles in bin  $i$  at time  $t$ . This allows us to observe the evolution of each system as well as the final state of each simulation after 1000 time steps.

Note that the agent based model (1) does not exactly replicate the predictions of the ODEs. In comparing the aggregation patterns

produced by the particle system to the ODE, we see a similar number of aggregations forming at approximately the same time. In the first example with persistence parameter  $a = 0.3$  and neighbor detection distance  $D = 10$ , four aggregations are formed over the 100 bins in both the stochastic and deterministic simulation. In Fig. 7, we see that the forming aggregations do not end in identical locations and they are not the same height. Still, the patterns are similar: their number is similar and they appear to be of approximately the same width. Similarly, for the parameter set with persistence probability  $a = 0.3$  and neighbor detection distance  $D = 20$ , we observe that the aggregation patterns match in number, width, and approximate height and location. The qualitative agreement appears to break down as  $a + b$  approaches 1, i.e., when the neighbor attractive force approaches zero.

In the case where no aggregations form, particles are seen to be distributed relatively uniformly, as observed in the 3D surface evolution plots in Fig. 6. Upon closer inspection of this distribution, as can be observed in Fig. 7, the particles actually form a wave, the shape of which depends on the parameters and the initial conditions. We initially expected that simulations without aggregations would produce a uniform distribution of particles; however, this only appears to be the case when  $a + b = 1$  and the initial data is uniformly distributed. We discuss this in more detail in the next

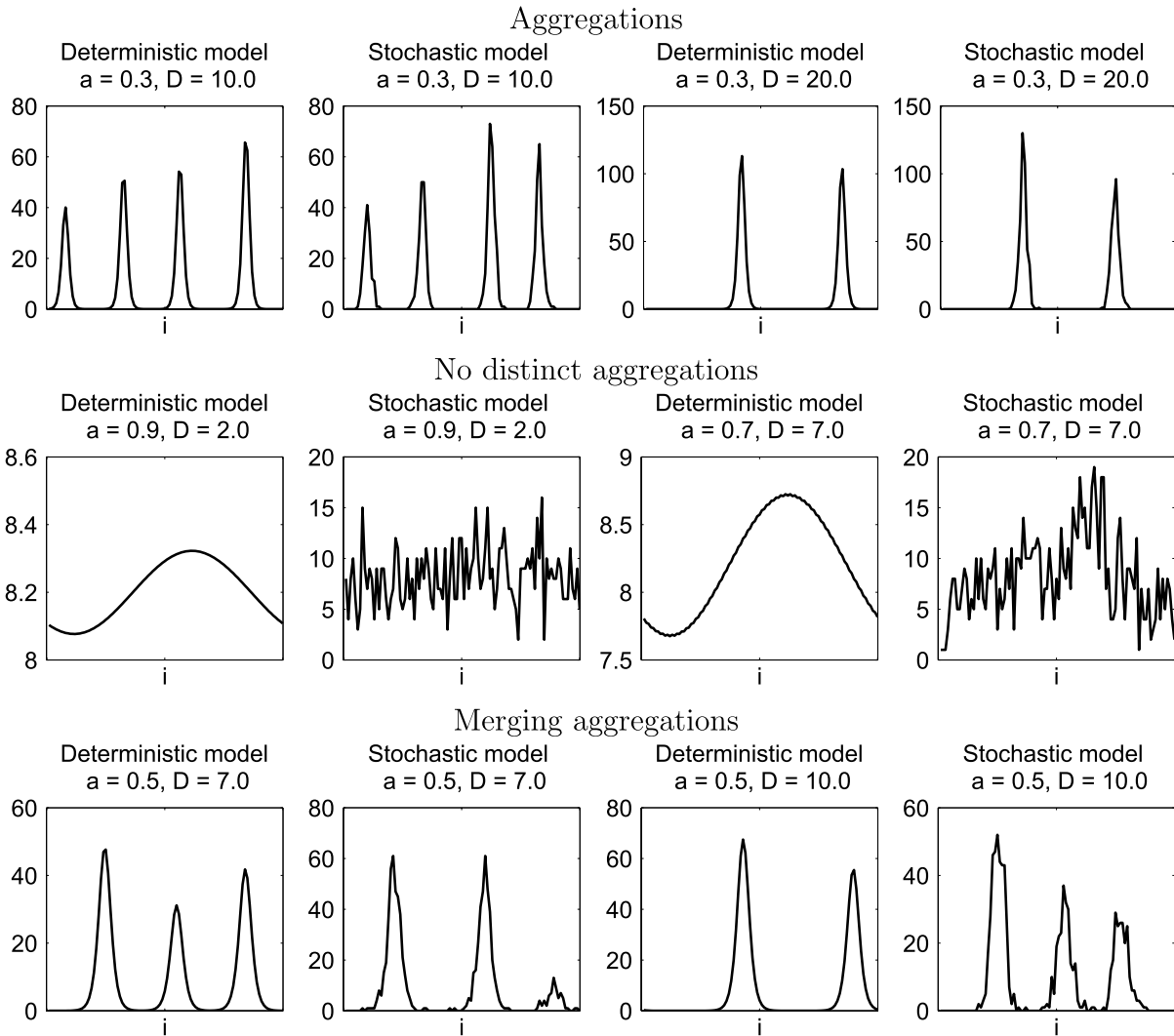


**Fig. 7.** Comparison of the stochastic particle system and the deterministic ODE for different scenarios: aggregations, the absence of aggregations, and merging aggregations at  $t = 1000$ . This figure corresponds to the final time of the simulations shown in Fig. 6. The parameters  $a$ , the persistence probability,  $D$ , the neighbor detection distance, and the initial data are the same in each case. The parameters  $a$  and  $D$  are varied as indicated above each plot to create the different scenarios. In all images, the stopping probability  $b$  is 0.1 and the number of slots  $k$  is 100. On these 2D plots, the  $i$ -axis is for bin number, ranging from 1 to 100 and the vertical  $z$ -axis is for the number of particles, specifically  $M_i(1000)$ .

section. In comparing the deterministic model and the stochastic model, we see that the stochastic model contains quite a lot of variation. Yet, the overall wave trend of the stochastic simulation seems to match the deterministic simulation. The variations in particle number for each bin illustrate the relatively large stochastic effect of the particle system. These effects become more important when looking at simulations with unstable dynamics.

In the last case of simulations with merging aggregations, the merging times and patterns are very sensitive to the exact number of particles in each location. In comparing the surface evolutions of the stochastic simulations to the deterministic simulations, we see that the aggregations do not merge at the same time and the larger (or smaller) aggregations are not in the same locations. However, we do observe that the general emerging patterns of particles are somewhat similar at the final time  $t = 1000$ , especially in the first merging aggregation example with  $a = 0.5$  and  $D = 7$ . In the second merging aggregation example with  $a = 0.5$  and  $D = 10$ , it appears as though the stochastic simulation will eventually form two large peaks, with the smaller peaks merging.

We further explore patterns of merging aggregations in Fig. 8, where we show four different instances of a simulation of the stochastic particle system with the same parameters ( $a = 0.5$ ,  $b =$

$0.1$ ,  $D = 7$ ) and initial conditions. In the simulation of the deterministic ODE model, there are initially four aggregations. Eventually, after approximately 900 time steps, two of these aggregations merge. Of the resulting three aggregations, there are two relatively tall peaks and one shorter peak. In contrast, in the four stochastic simulations, three simulations yield similar results with three peaks, two tall and one short, at  $t = 1000$ . The simulation with four peaks at  $t = 1000$  appears as though aggregations would be likely to merge shortly after this time. In the stochastic model, the initial data seem to converge quickly to five aggregations, two of which in each image merge almost immediately. Immediate merging of two small aggregations may explain how the taller peak in the deterministic model developed.

While a wide variation in the exact positions and heights of aggregations is observed in many simulations, we also observe qualitatively similar general patterns, such as aggregation number and peak width, emerging under similar conditions. Due to the wide variation in patterns and the length of time to run each stochastic simulation (varying from 2 to 10 min depending on our choice of parameters), we have chosen not to perform a Monte Carlo simulation to confirm that the average behavior of the stochastic simulation does in fact match the system of ODEs.

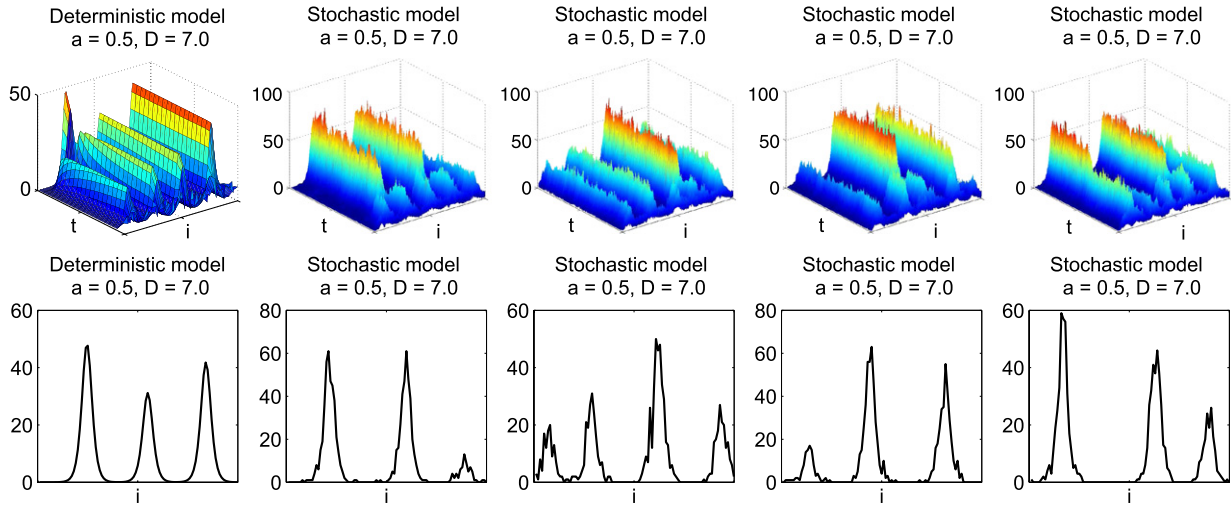


**Fig. 8.** Four simulations of the stochastic model for the same parameter set, alongside the simulation produced by the deterministic ODE model. In all images, the persistence probability  $a$  is 0.5, the neighbor detection distance  $D$  is 7, the stopping probability  $b$  is 0.1, and the number of bins  $k$  is 100. On the 3D plots, the  $i$ -axis is for bin number, ranging from 1 to 100, the  $t$ -axis is for time step, from 1 to 1000, and the vertical  $z$ -axis is for total particle number,  $M_i(t)$ . On the 2D plots, the  $i$ -axis is for bin number and the vertical  $z$ -axis is for total particle number at the final time  $t = 1000$ .

We are able to extract critical information from the system without performing this calculation.

### 3.2. Uniform initial conditions

Before considering more simulations of this model, let us make a few observations about the model (17)–(20). Suppose each bin contains the same number,  $x$ , of right-moving particles and the same number,  $y$ , of right-stationary and left-stationary particles. Upon substitution, we observe that the total number of particles,  $M_i(t) = R_i(t) + R_i^s(t) + L_i(t) + L_i^s(t)$ , is constant in time. Furthermore, the moving and stationary populations are also at a steady state if  $x = \frac{1-b}{b}y$ . Hence we expect that for uniform initial conditions, with the same number of particles in each bin and equal left- and right-moving (and stationary) particles, the total number of particles will remain constant with a uniform distribution.

We check this steady state in the following numerical simulation. In Fig. 9, we illustrate simulations where each particle-type-bin combination contains 2 particles, for a total of 8 particles in each bin. The simulations are run for combinations of parameters varying the persistence probability  $a$  and stopping probability  $b$  through a set of values (0.1, 0.3, 0.5, 0.7, 0.9). Note that  $a + b \leq 1$  is a hard constraint on the system; that is, the particles can either persist, stop or choose a new direction, but they cannot perform more than one of these actions at a time. Observe that these simulations suggest that a uniform distribution of particles is an unstable steady state of the system. We confirmed the numerical instability of the uniform solution by using stricter error tolerances of numerical integration in MATLAB. In doing so, we observed that the solution takes more time to diverge from the steady state. Additionally, there was a noticeable delay in aggregation formation, and we observed a shift in the location of the aggregations.

### 3.3. Parameter analysis by simulation

We continue our study by considering the case of initial conditions that follow a Poisson distribution. We generated a set of initial data with a Poisson distribution with mean 2 for each population type and bin. We use the same set of initial data for each simulation. The total number of particles for each bin, as well

as a break down of particle number by population, are shown in Fig. 10. The total number of particles in this example is 820.

In comparing simulations for this initial data set, our objective is to better understand the effect of each parameter and their interdependencies. We begin by considering the effect of varying both the persistence probability  $a$  and the stopping probability  $b$ . Each probability can vary between 0 and 1. In varying both parameters, we are constrained by  $a + b \leq 1$ : the probability of persisting, stopping, and changing directions based on neighbor-weights must add up to one. In Fig. 11, we show the distribution of particles at the final time 1000. In both figures, the parameters  $a$  and  $b$  are chosen from the set {0.1, 0.3, 0.5, 0.7, 0.9}. We observe that as the persistence probability  $a$  is increased, the number of aggregations decreases. A similar trend occurs with the stopping probability. As  $b$  increases, the number of aggregations decreases; however, this relationship appears to also depend on the value of  $a$ . The dependence of the number of aggregations on persistence probability  $a$  is stronger than the dependence on the stopping probability  $b$ . Note that for  $a = 0.1$ , for this set of parameters, the only effect of increasing  $b$  appears to be in the increased width of the peaks, as shown in Fig. 11. The width of peaks also increases with increased persistence probability  $a$ . We also observe, for images with  $a + b = 1$  in Fig. 11, that the magnitude of these waves decreases for an increase in the persistence probability  $a$ . Further, note that a few of the simulations do not appear to have reached a steady state, e.g., parameter sets  $(a, b) = (0.3, 0.5)$  and  $(0.7, 0.1)$ , where nonzero dips between peaks appear as a viable source of merging aggregations.

We next study the relation between the parameters  $a$ , the persistence probability, and  $D$ , the neighbor detection distance. To do this, we again allow  $a$  to take values in the set {0.1, 0.3, 0.5, 0.7, 0.9}. We consider two ranges of values for  $D$ : {2, 5, 10, 20, 40} and {1, 3, 5, 7, 9}. The first range allows us to consider the large scale effects of doubling the parameter  $D$ . The second range allows us to consider the effect of varying parameter  $D$  by relatively small increments. The second range is more likely the biologically reasonable range to consider, but understanding the larger scale effects of  $D$  is also important. We set the stopping probability  $b = 0.1$ . Results are shown in Figs. 12–13. The snapshot of the distribution of particles is taken at the final time  $t = 1000$ . The number of bins equals 100. Once again, increasing the persistence probability  $a$  clearly decreases the number of ag-

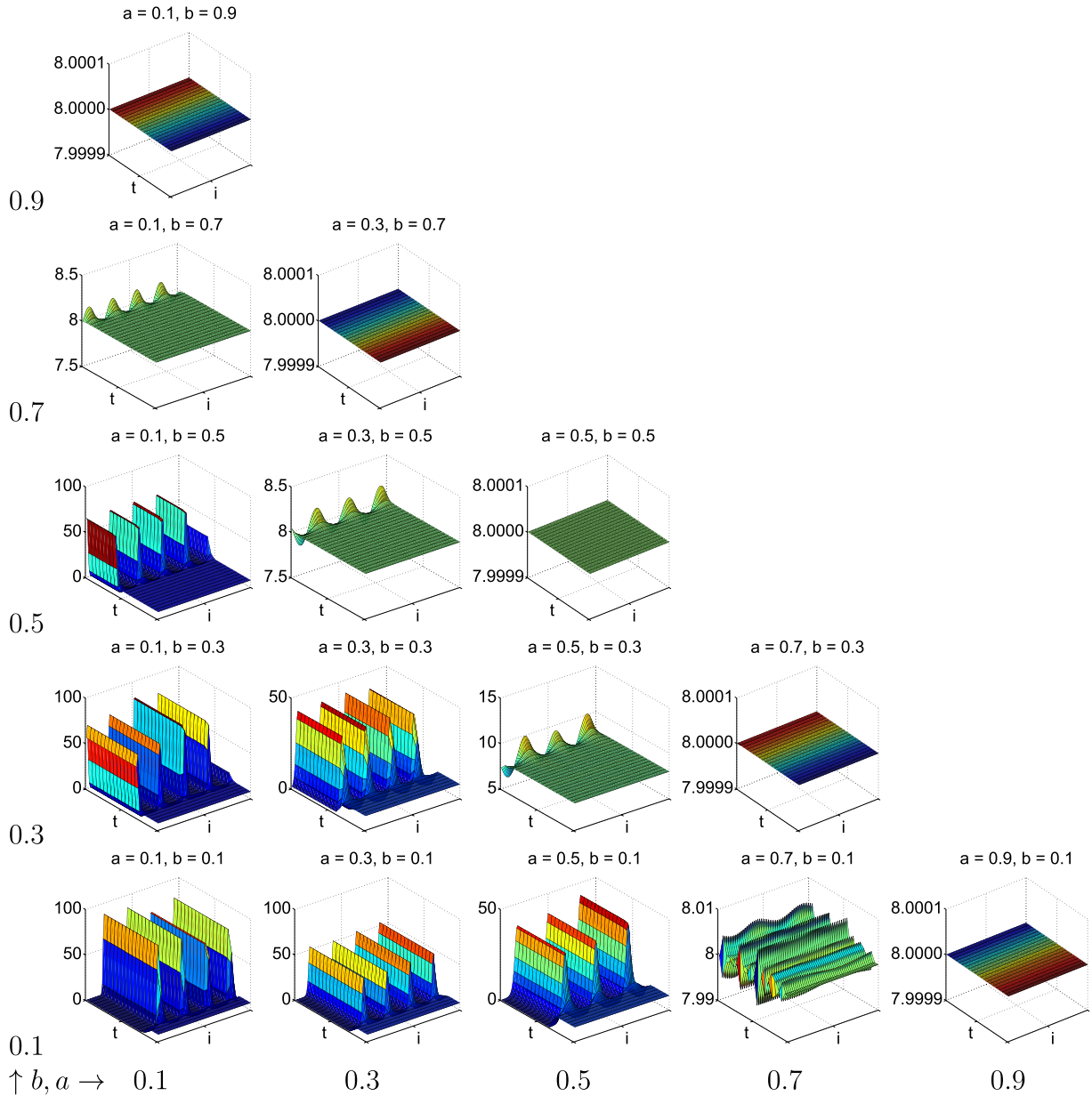


**Fig. 9.** Exploration of parameter space for parameters  $a$ , the persistence probability, and  $b$ , the stopping probability, for uniform initial conditions ( $M_i(0) = 8$  for all  $i$ ). Note that there is a hard constraint that  $a + b \leq 1$ . For cases where  $a + b = 1$ , particles do not have the ability to choose to move in a new direction; they can only stop or persist in their initially preferred direction. In all cases, the interaction distance  $D$  is 10 and the number of bins  $k$  is 100. The  $i$ -axis is the bin number, ranging from 1 to 100, the  $t$ -axis is for time, from 1 to 1000, and the vertical  $z$ -axis is for total particle number,  $M_i(t)$ .

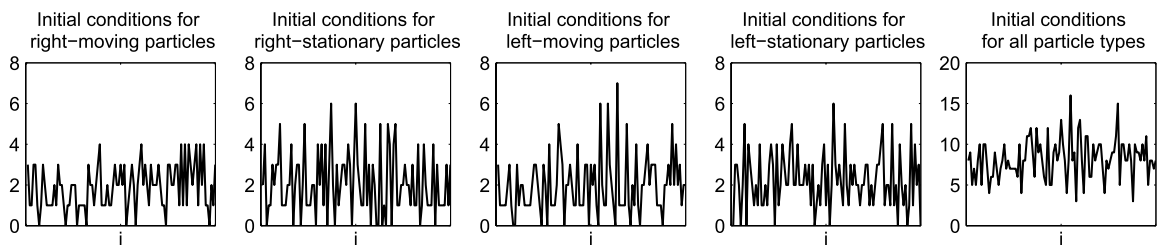


**Fig. 10.** Initial conditions for Figs. 11–15. The first four plots, for right-moving  $R_i^r(0)$ , right-stationary  $R_i^s(0)$ , left-moving  $L_i^l(0)$  and left-stationary  $L_i^s(0)$  are used to initiate the ODEs (and the stochastic systems in Figs. 6–8). The last plot is the sum of these four plots,  $M_i(0)$  and is what is visible in subsequent images. Particle numbers are distributed with a Poisson distribution with mean 2 for each population type in each bin  $i$ . The  $i$ -axis varies from 0 to 100. The total number of particles is 820.

gregations and increases the width of aggregation peaks. Increasing the neighbor detection distance  $D$  also decreases the number of aggregations. Interestingly, the neighbor detection distance  $D$  does

not appear to affect the width of aggregations. In Fig. 12, we notice that doubling the interaction distance yields approximately half as many aggregations. In Figs. 12–13, when the persistence proba-

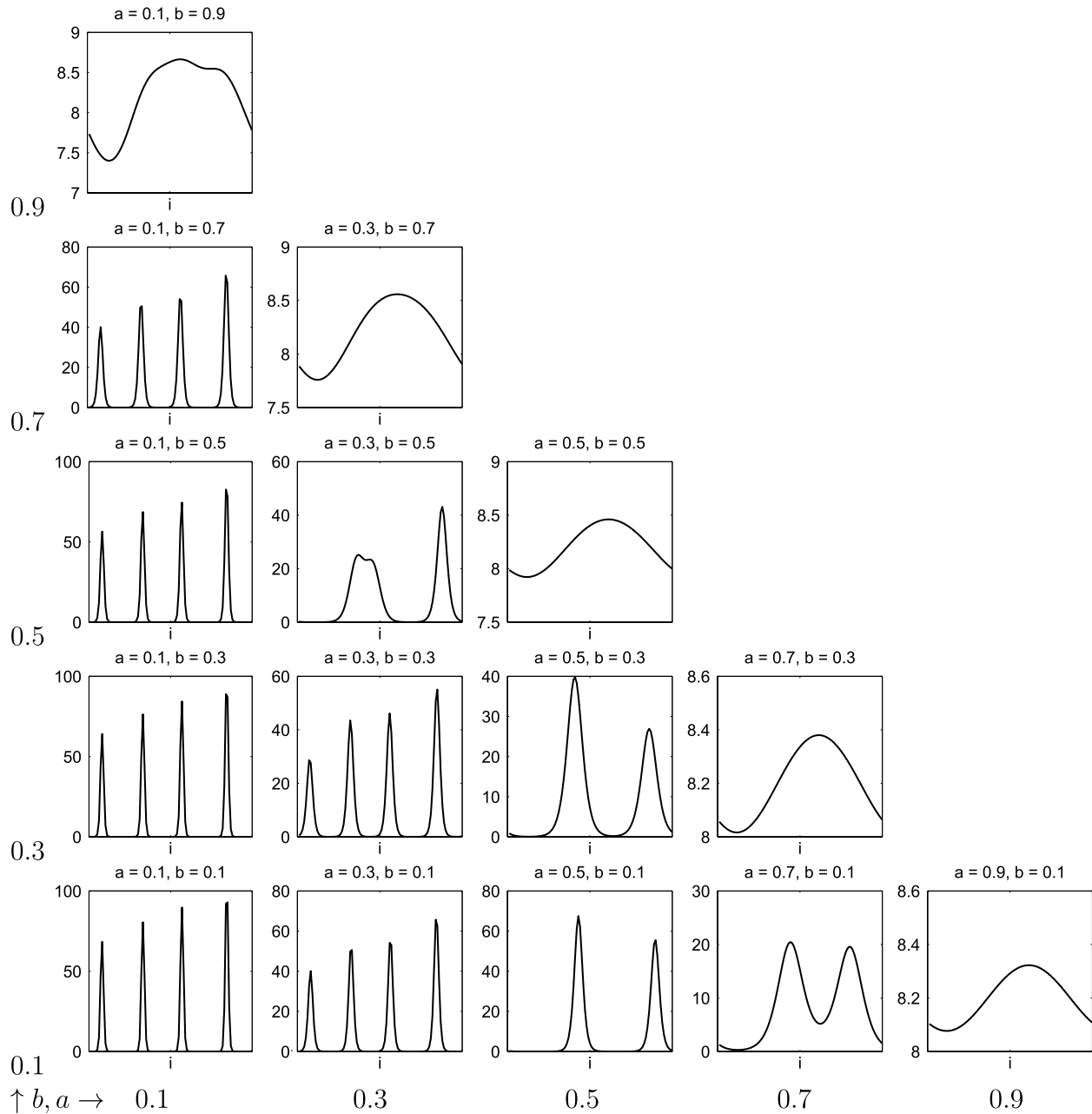


**Fig. 11.** The final distribution at time  $t = 1000$  of the simulations in exploration of the parameter space for parameters  $a$ , the persistence probability, and  $b$ , the stopping probability. Note that  $a + b \leq 1$ . For cases where  $a + b = 1$ , particles cannot change their direction; they can only stop or persist in their initially preferred direction. In all cases, the interaction distance  $D$  is 10 and the number of bins is 100. The  $i$ -axis is for the bin number and the vertical  $z$ -axis is for particle number. The initial conditions are given in Fig. 10.

bility is  $a = 0.7$ , the system develops harmonic frequencies for a neighbor detection distance  $D$  that is between 1 and 5. When this occurs, the magnitude of the wave (in the absence of aggregations) becomes very small. Fig. 13 also illustrates that the number of aggregations is very sensitive to  $D$  for very low values of  $D$ , but not very sensitive for values of  $D$  larger than 5.

Finally, we explore the dependencies between the stopping probability  $b$  and the neighbor detection distance  $D$ . For these simulations, we set the persistence probability  $a$  to 0.3 which results in a more interesting dynamics compared with the case when  $a = 0.1$ . The stopping probability  $b$  takes values in  $\{0.1, 0.3, 0.5, 0.7\}$ . Two sets of values are considered for  $D : \{2, 5, 10, 20, 40\}$  and  $\{1, 3, 5, 7, 9\}$ . The results are shown in Figs. 14–15. Clearly, for the larger range of  $D$  values, shown in Fig. 14, the stopping probability  $b$  only affects the simulations

when  $b \geq 0.5$ . This is most likely due to our choice of the persistence parameter  $a$ . Once again it is observed that if the detection distance  $D$  is doubled, the number of aggregations is approximately halved. For  $b = 0.7$ , where  $a + b = 1$ , we observe the same wave pattern to what was seen in Figs. 11–13. Similar results are obtained for low values of  $D$ , as can be seen in Fig. 15.

There are a few interesting artifacts of these simulations that may be related to our choice of initial data set. The aggregations appear in approximately the same location in every simulation. This is very notable for simulations with one or two peaks. Additionally, in cases of two aggregations, the relative size of the peaks almost always decreases with increasing bin number. Similarly, for cases with four aggregations, the relative height of the peaks increases with an increasing bin number. Furthermore, for cases with no aggregations, the resulting wave is in approximately the same

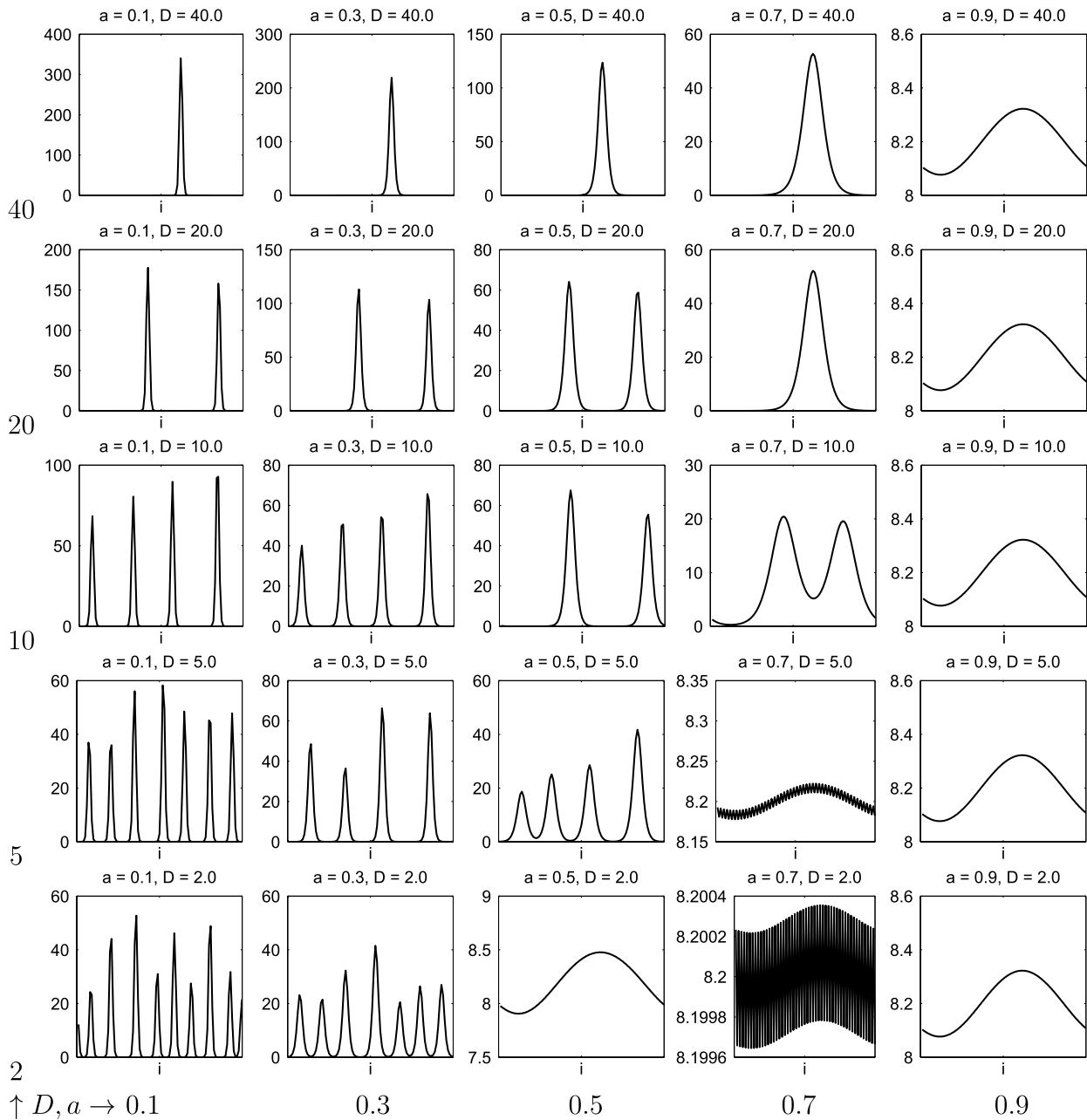


**Fig. 12.** The final distribution at time  $t = 1000$  of the simulations in exploration of the parameter space for parameters  $a$ , the persistence probability, and  $D$ , the neighbor detection distance. In all images, the stopping probability  $b$  is 0.1 and the number of bins is 100. The  $i$ -axis is for the bin number, from 1 to 100, and the vertical  $z$ -axis is for the particle number. The initial conditions are given in Fig. 10.

phase for each simulation, although the magnitude varies. Comparing these situations to the set produced with uniform initial data, the latter yields shifted sets of peaks for differing simulations.

#### 4. Discussion

Comparing simulations from our stochastic model [1,2] to the ODE model (17)–(20), illustrates that the general trends in both models are the same. These trends include the number of aggregations, the width and height of these peaks, and the dynamics of merging aggregations.

For a constant uniform initial distribution of particles, we showed that while the ODE system is supposed to be at steady state, the numerical simulations suggest that this is an unstable steady state. This reveals itself in numerical simulations where

integration error accumulates, eventually causing the presence of aggregations, though we expect a constant uniform steady state. Changing the numerical integration error tolerances has a small effect on the temporal appearance and location of aggregations produced by small disturbances due to integration error.

We analyzed the parameter space by considering a set of random initial conditions with a Poisson distribution, with which we were able to examine the complex interplay between the persistence probability  $a$ , the stopping probability  $b$ , and the neighbor detection distance  $D$ . In considering the parameters individually, we note that increasing the persistence parameter  $a$  decreases the number of aggregations and increases the width of peaks. The effect of increasing the stopping probability  $b$  is a decrease in the number of aggregations and an increase in the width of aggregations. We observed that increasing  $a$  and  $b$

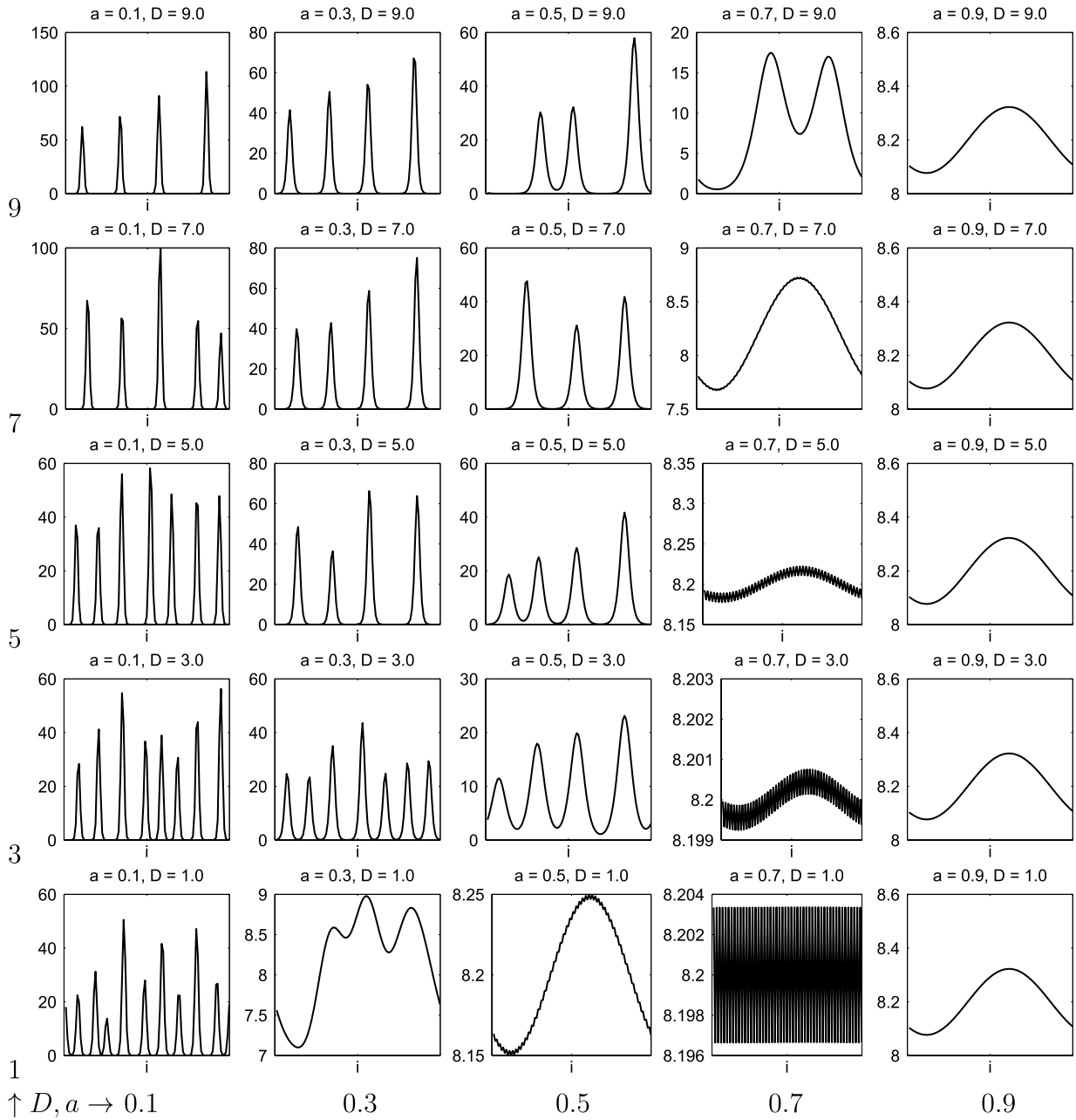


**Fig. 13.** The final distribution at time  $t = 1000$  of the simulations in exploration of the parameter space for parameters  $a$ , the persistence probability, and  $D$ , the neighbor detection distance. In all images, the stopping probability  $b$  is 0.1 and the number of bins is 100. The  $i$ -axis is for bin number, ranging from 1 to 100, and the vertical  $z$ -axis is for the particle number. The initial conditions are given in Fig. 10.

effectively decreases the probability of a particle being able to change directions in order to move toward a neighbor. In this way, particles are unable to form as tight of aggregations and instead form less, yet larger peaks. Increasing the neighbor detection distance  $D$  decreases the number of peaks but does not affect the width of peaks; instead, it appears to affect the height of such peaks. Note that changing  $D$  does not change the total probability with which a particle can choose to move in a new direction, and  $a$  and  $b$  remain fixed. In this way, the width of peaks is not affected. Furthermore, doubling  $D$  appears to halve the number of these aggregations. We expect that for neighbor detection distances exceeding half the total number of available bins, there will either be one or no aggregations. In such a system, all particles are able to sense all other particles.

We also observed that when particles are only capable of persisting in their current direction or stopping, maintained by

the constraint  $a + b = 1$ , the deterministic result appears to be periodic, with the shape of the curve depending on the general shape of the initial data. These results also occur for parameter sets where  $a + b$  is close to one and the neighbor detection distance  $D$  is relatively small.

### 5. Conclusions

In this paper, we consider a system of particles that interact in one space dimension according to the rules of our stochastic model in [1,2]. In the stochastic system, particles are allowed to (i) interact by moving in the direction of a randomly selected neighbor, within some defined neighbor detection distance, (ii) persist in their motion (memory), or (iii) become stationary (or start moving). These simple group dynamics produce many complex structures that have not been previously studied. We use these dynamics

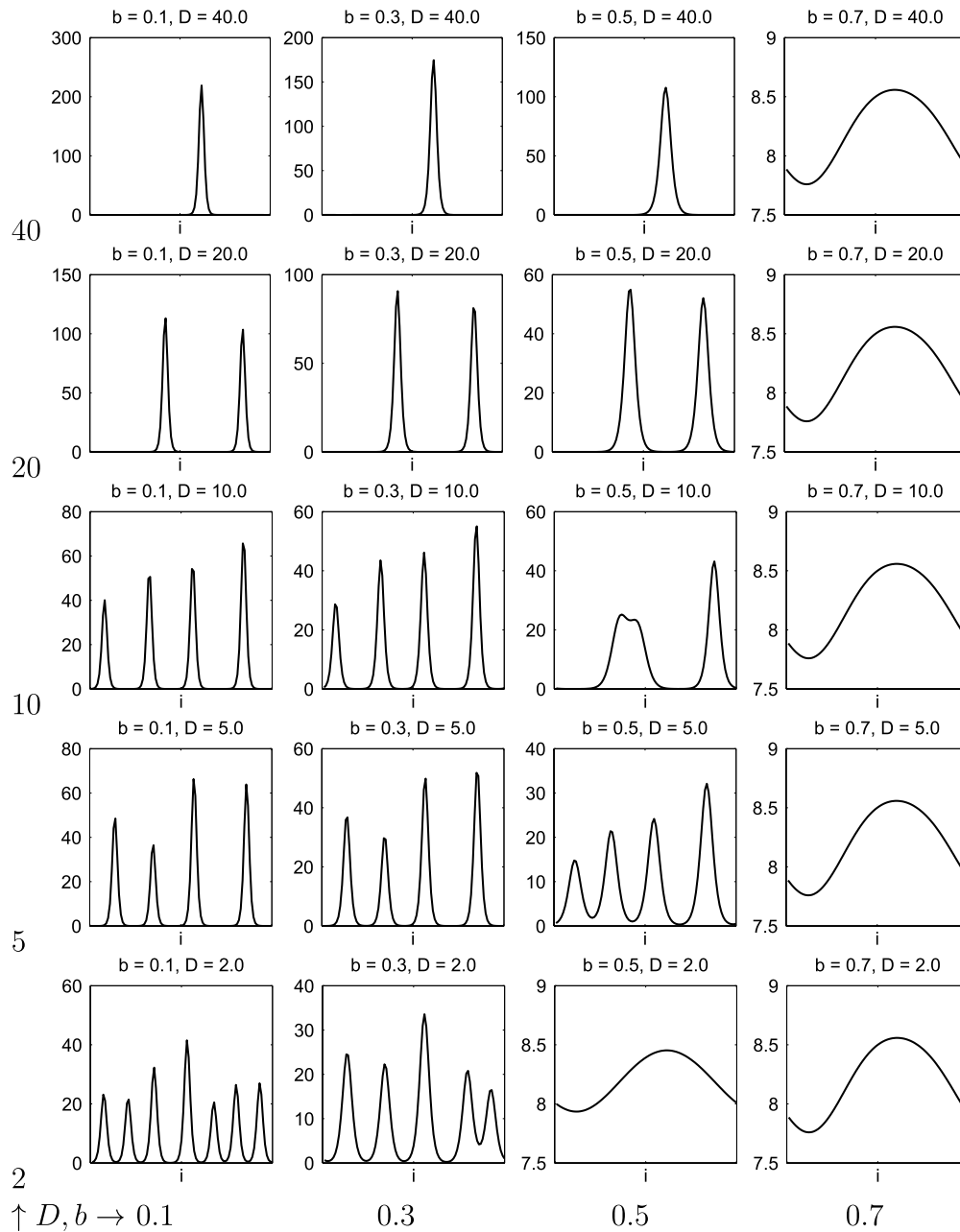


**Fig. 14.** The final distribution at time  $t = 1000$  of the simulations in exploration of the parameter space for parameters  $b$ , the persistence probability, and  $D$ , the neighbor detection distance. In all images, the stopping probability  $a$  is 0.3 and the number of bins is 100. The  $i$ -axis is for the bin number, from 1 to 100, and the vertical  $z$ -axis is for the particle number. The initial conditions are given in Fig. 10.

to develop a system of ODEs that follows the distribution of particles along the line. The ODEs allow us to effectively explore the parameter space. We perform numerous simulations with varying parameter sets and initial conditions. The simulations produce a variety of scenarios such as aggregations of cells and instabilities that result in merging aggregations. The simulations replicate key characteristics of the stochastic particle model. The results correspond to characteristics of the experimentally observed motion of bacteria.

The biological implications of this study motivate some future research directions. We expect the neighbor detection distance, which may be related to the biological setup (the length of pili on the surface of cyanobacteria or the diffusion length scale of signaling molecules) to vary from particle to particle. The stopping and persistence probabilities may also vary from particle to parti-

cle, and the values most likely span over a wide range, depending on temporal characteristics (e.g., how many polysaccharides the particles have produced and how many of them are present in the agarose). These characteristics can be incorporated in future work.

Mathematically, this model lends itself to further analysis, by way of derivation of a partial differential equation. It is likely that deriving such a model would produce an integro-differential equation, with integrals being used to account for neighbors within fixed distances of the particle. Furthermore, the ODE model can be extended to two dimensions, which is of interest, yet outside of the scope of this paper.

#### Acknowledgments

This work was supported in part by the joint NSF/NIGMS program under Grant No. DMS-0758374 and in part by Grant No.

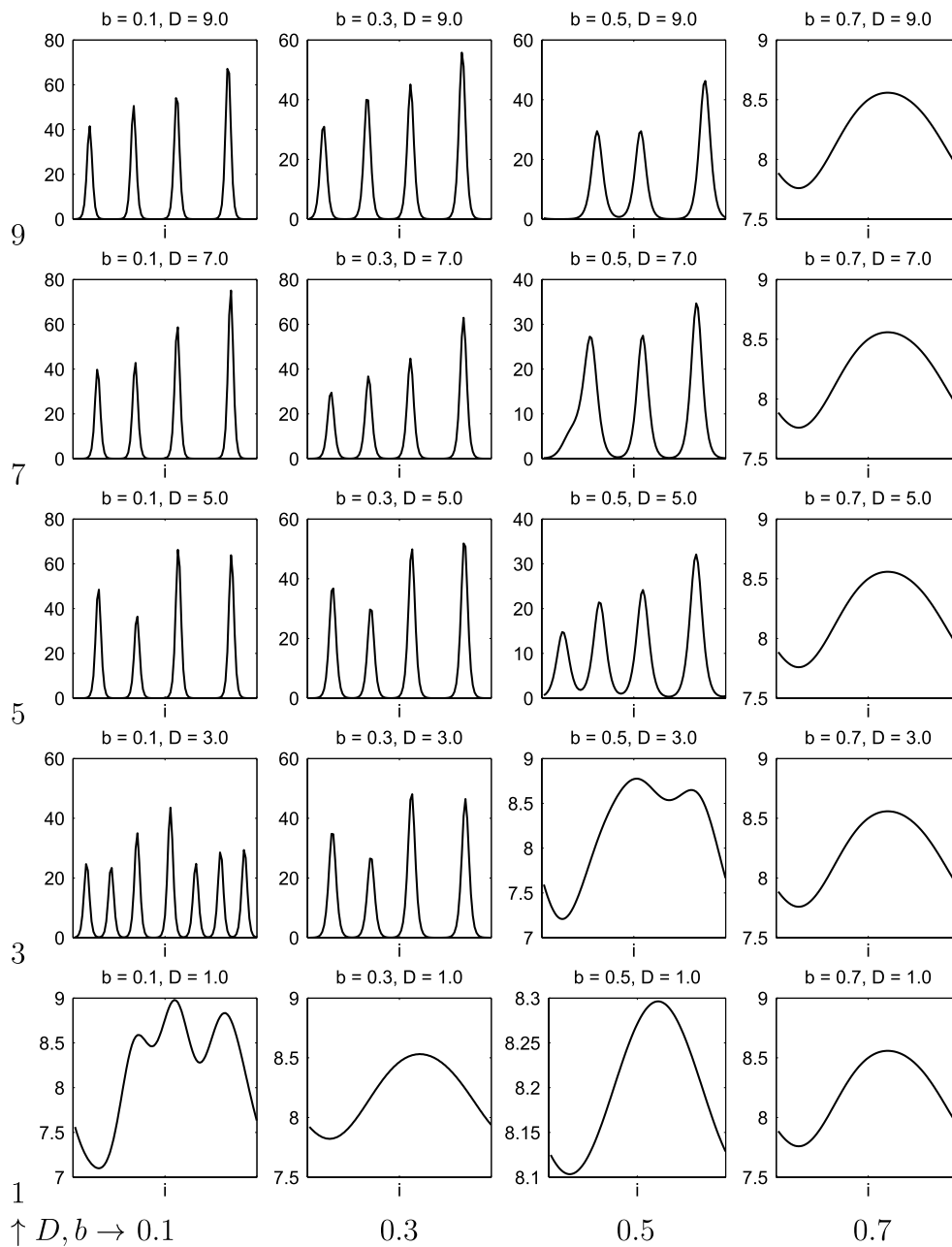


**Fig. 15.** The final distribution at time  $t = 1000$  of the simulations in exploration of the parameter space for parameters  $b$ , the persistence probability, and  $D$ , the neighbor detection distance. In all images, the stopping probability  $a$  is 0.3 and the number of bins  $k$  is 100. The  $i$ -axis is for bin number, from 1 to 100, and the vertical  $z$ -axis is for the particle number. The initial conditions are given in Fig. 10.

R01CA130817 from the National Cancer Institute. The content is solely the responsibility of the authors and does not necessarily represent the official views of the National Cancer Institute or the National Institutes of Health.

## References

- [1] A. Galante, S. Wisen, D. Bhaya, D. Levy, Stochastic models and simulations of phototaxis, in: H. Sayama, A.A. Minai, D. Braha, Y. Bar-Yam (Eds.), *Unifying Themes in Complex Systems Volume VIII: Proceedings of the Eighth International Conference on Complex Systems*, in: *New England Complex Systems Institute Series on Complexity*, NECSI Knowledge Press, Boston, MA, 2011, pp. 105–119.
- [2] A. Galante, S. Wisen, D. Bhaya, D. Levy, Modeling local interactions during the motion of cyanobacteria, *J. Theoret. Biol.* 309 (2012) 147–158.
- [3] D. Bhaya, Light matters: phototaxis and signal transduction in unicellular cyanobacteria, *Molecul. Microbiol.* 53 (2004) 745–754.
- [4] M. Burriesci, D. Bhaya, Tracking phototactic responses and modeling motility of *synechocystis* sp. Strain PCC6803, *J. Photochem. Photobiol. B* 91 (2008) 77–86.
- [5] I.D. Couzin, J. Krause, R. James, G.D. Ruxton, N.R. Franks, Collective memory and spatial sorting in animal groups, *J. Theoret. Biol.* 218 (2002) 1–11.
- [6] T. Vicsek, A. Czirók, E. Ben-Jacob, I. Cohen, O. Shochet, Novel type of phase transition in a system of self-driven particles, *Phys. Rev. Lett.* 6 (1995) 1226–1229.
- [7] P. Degond, S. Motsch, Continuum limit of self-driven particles with orientation interaction, *Math. Models Methods Appl. Sci.* 18 (2008) 1193–1215.
- [8] F. Cucker, S. Smale, On the mathematics of emergence, *Jpn. J. Math.* 2 (2007) 197–227.
- [9] F. Cucker, S. Smale, Emergent behavior in flocks, *IEEE Trans. Automat. Control* 52 (2007) 852–862.
- [10] S.Y. Ha, E. Tadmor, From particle to kinetic and hydrodynamic descriptions of flocking, *Kinet. Relat. Models* 1 (3) (2008) 415–435.
- [11] I. Aoki, A simulation study on the schooling mechanism in fish, *Bull. Japan Soc. Fish.* 48 (8) (1982) 1081–1088.
- [12] A. Huth, C. Wissel, The simulation of movement of fish schools, *J. Theoret. Biol.* 156 (3) (1992) 365–385.

- [13] Y.X. Li, R. Lukeman, L. Edelstein-Keshet, Minimal mechanisms for school formation in self-propelled particles, *Physica D* 237 (2008) 699–720.
- [14] R. Lukeman, Y.X. Li, L. Edelstein-Keshet, Inferring individual rules from collective behavior, *Proc. Natl. Acad. Sci.* 107 (2010) 12576–12580.
- [15] J.K. Parrish, S.V. Viscido, D. Grunbaum, Self-organized fish schools: an examination of emergent properties, *Biol. Bull.* 202 (2002) 296–305.
- [16] E.F. Keller, L.A. Segel, Model for chemotaxis, *J. Theoret. Biol.* 30 (2) (1971) 225–234.
- [17] C.S. Patlak, Random walk with persistence and external bias, *Bull. Math. Biophys.* 15 (1953) 311–338.
- [18] M.S. Alber, M.A. Kiskowski, J.A. Glazier, Y. Jjiang, On cellular automaton approaches to modeling biological cells, in: D.N. Arnold, F. Santosa (Eds.), *Mathematical Systems Theory in Biology, Communication, and Finance*, in: IMA, vol. 134, Springer-Verlag, New York, 2002, pp. 1–40.
- [19] T. Hillen, K.J. Painter, A users guide to PDE models for chemotaxis, *J. Math. Biol.* 57 (2009) 183–217.
- [20] D. Horstmann, From 1970 until present: the Keller–Segel model in chemotaxis and its consequences I, *Jahresberichte DMV* 105 (3) (2003) 103–165.
- [21] H.G. Othmer, T. Hillen, The diffusion limit of transport equations II: chemotaxis equations, *SIAM J. Appl. Math.* 62 (4) (2002) 1222–1250.
- [22] M.J. Tindall, P.K. Maini, S.L. Porter, J.P. Armitage, Overview of mathematical approaches used to model bacterial chemotaxis II: bacterial populations, *Bull. Math. Biol.* 70 (2008) 1570–1607.
- [23] U. Burkhardt, D.P. Hader, Phototactic attraction in light trap experiments: a mathematical model, *J. Math. Biol.* 10 (1980) 257–269.
- [24] A.F.M. Maree, A.V. Panfilov, P. Hogeweg, Phototaxis during the slug stage of *Dictyostelium discoideum*: a model study, *Proc. R. Soc. Lond. Ser. B* 266 (1999) 1351–1360.
- [25] H. Fatehi, M. Meyer-Hermann, M.T. Figge, Modelling cellular aggregation induced by chemotaxis and phototaxis, *Math. Med. Biol.* 27 (2010) 373–384.
- [26] K. Drescher, R.E. Goldstein, I. Tuval, Fidelity of adaptive phototaxis, *Proc. Natl. Acad. Sci.* 107 (25) (2010) 11171–11176.
- [27] D. Bhaya, D. Levy, T. Requeijo, Group dynamics of phototaxis: interacting stochastic many-particle systems and their continuum limit, in: S. Benzoni-Gavage, D. Serre (Eds.), *Hyperbolic Problems: Theory, Numerics, Application (Proceedings of HYP 2006, Lyon, France)*, Springer-Verlag, Berlin, 2008, pp. 145–169.
- [28] D. Levy, T. Requeijo, Modeling group dynamics of phototaxis: from particle systems to PDEs, *Discrete Contin. Dyn. Syst. Ser. B* 9 (2008) 103–128.
- [29] D. Levy, T. Requeijo, Stochastic models for phototaxis, *Bull. Math. Biol.* 70 (2008) 1684–1706.
- [30] D. Levy, S.Y. Ha, Particle, kinetic and fluid models for phototaxis, *Discrete Contin. Dyn. Syst. Ser. B* 12 (2009) 77–108.
- [31] R.E. Baker, C.A. Yates, R. Erban, From microscopic to macroscopic descriptions of cell migration on growing domains, *Bull. Math. Biol.* 72 (2010) 719–762.
- [32] R. Erban, S.J. Chapman, P. Maini, A practical guide to stochastic simulations of reaction–diffusion processes, 2007, p. 34. Available as: <http://arxiv.org/abs/0704.1908>.